Inverse Calculation of Time-Spatial Varying Mold Heat Flux During Continuous Casting from Fast Response Thermocouples

Haihui Zhang, Huiqiang Shen, and Pengcheng Xiao

Abstract This paper covers the determination of time-spatial varying mold heat flux using mold temperatures measured by fast response thermocouples at a frequency up to 60 Hz. A two-dimensional transient inverse heat conduction problem (2DIHCP) is established, where 2DIHCP is developed based on the sequential function specification method implemented with the spatial regularization terms to reduce the fluctuations in the estimated heat flux in both time and spatial domain. Then, the inverse problem was validated using a designed numeric test-problem. Finally, the inverse problem is applied to calculating the heat flux across the mold hot surface for a continuous casting trial using the mold simulator.

Keywords Modeling and simulation · Iron and steel · Process technology · Continuous casting

Nomenclature

c	Heat capacity (J/kg K)
$f(\partial\Omega_4, t)$	Temperature of the boundary $\partial\Omega_4$ (K)
$\mathbf{H}$	Spatial regularization matrix
$\mathbf{X}$	Sensitivity matrix
M	Numbers of the thermocouple in the calculated domain Ω
n_j	Number of heat flux components at the boundary $\partial\Omega_j, j = 1, 2, 3.$
N	$N = n_1 + n_2 + n_3$
q	Heat flux (W/m^2)

H. Zhang (✉) · H. Shen
Faculty of Materials Metallurgy and Chemistry, Jiangxi University of Science and Technology, Ganzhou 341000, China
e-mail: zhanghaihuiemail@gmail.com

P. Xiao
College of Metallurgy and Energy, North China University of Science and Technology University, Tangshan 063210, China

r	Future time step $(-)$
s	Objective function
t, t_j	Time (s)
$\mathbf{T}$	Vector of estimated temperature (K)
T_m	Estimated temperatures at the measurement location (x_m, y_m) (K)
T_{ini}	Initial temperature (K)
x, y	Cartesian spatial coordinates (m)
$\mathbf{Y}$	Vector of the measured temperature (K)
Y_m	Measured temperature at the measurement location (x_m, y_m) (K)

Greek Symbols

α	Regularization parameters ($K^2 \, m^4 \, W^4$)
λ	Thermal conductivity ($W \, m^{-1} \, K^{-1}$)
ρ	Density ($kg \, m^{-3}$)
σ	Standard deviation of the measurements
ω	Random variable
Ω	Calculated domain
$\partial\Omega_1, \partial\Omega_2, \partial\Omega_3, \partial\Omega_4$	Boundary of the calculated domain Ω

Introduction

Many surface defects in final rolled steel products originate from the initial solidification of molten steel inside continuous casting molds. This has been found to be associated with the heat transfer behaviors of the mold itself [1–3]. The mold heat flux, especially at the mold meniscus area, is extremely complex due to the transient nature of the infiltration of lubricant liquid mold flux, intensive fluid flow, and mold oscillation, such that it would be very difficult to get a clear comprehensive understanding of all dynamics within the system [4–8].

The heat flux of the mold is a space–time varying variable [9]. Usually, the mold heat transfer is monitored by temperature sensors [10]. Hundreds of thermocouples/sensors are employed to monitor the mold temperature during the continuous casting process, with a temperature sampling rate of 1–65 Hz. The mold heat flux cannot be calculated directly from the measured temperatures because of the lack of information on the boundary conditions. Mathematically, the determination of the mold heat flux from measured temperatures is an inverse problem that means the solution is usually unstable, not unique or does not exist, and a small measured error in the temperatures will result in a large error of heat flux [11, 12].

The inverse problem method has a broad application prospect in determining the heat flux from measured temperatures. The principle of inverse problems for restructuring the heat flux is to find out a heat flux with the maximum probability making the sum of squared deviations between the calculated temperatures **T** and the measured temperatures **Y** to be minimum [13].

The development of the use of inverse problem methods to calculate continuous casting mold heat flux from temperature measurements can be traced back to the works by Brimacomb et al. [14], followed by Thomas et al. [15], Wang et al. [16–18], Griffiths [19], Rajaraman [20], and Talukdar et al. [21]. Those inverse problem methods could be classified as the gradient-based type methods, such as the function specification method [9], the Tikhonov regularization [22] and the conjugate gradient method [23, 24], and the stochastic-based type methods, such as the genetic algorithm and the neural network algorithm [25]. However, the major weakness of the inverse problem persists in that it is extremely sensitive to temperature measurement errors, particularly as the time step is made smaller [12, 26]. As continuous casting technology progresses, fast mold thermal monitoring systems are adopted that could provide a more accurate detection precision supervising the fluctuation of mold temperature [5, 6]. However, the faster temperature sampling rate of mold thermal monitoring systems is inevitably accompanied by a higher intensity of the error/noise in the measured temperatures [12]. As a result of the increase of the temperature sampling rate, the use of small-time step frequently introduces instabilities in the solution of the inverse heat conduction problem.

In the engineering community, the inverse problem of Beck's sequential function specification method is well-known and very successfully used in solving inverse heat conduction problems for over 50 years [27–31]. For Beck's sequential function specification method, the heat flux form is assumed to be a constant function or a linear function over several future time steps due to the fact that the temperature response is lagging with respect to the boundary heat flux [23], then the stabilization of the solution in the time domain can be improved by choosing an appropriate number of future time steps [24, 32]. However, a common issue raised is how to improve the stabilization of the solution in the time and spatial domain for extending the sequential function specification method to the two-dimensional heat transfer problem [33, 34].

Therefore, the purpose of this work is to establish a two-dimensional transient **i**nverse **h**eat **c**onduction **p**roblem (2DIHCP) for the estimation of the mold heat flux from fast-sampled temperature data. The inverse problem is developed where the function specification method with a spatial Tikhonov regularization [6, 35, 36] was used to improve the stabilization of the solution in time and spatial domains, respectively. Then, a numeric test-problem was designed to validate the inverse problem. Finally, the inverse problem is applied to calculating the mold heat flux during liquid steel casting.

The Experimental and Direct Problem Description

The continuous casting trial was conducted using a mold simulator. As Fig. 1 shows, the mold simulator applied to this study is an inverse type water-cooled copper mold (30 mm × 50 mm × 350 mm) with oscillation capability. A U-shaped type water-cooling groove with a diameter of 10 mm is manufactured along the center line of mold plate, 12.5 mm away from both ends and gets connected 20 mm above the bottom, where the water flows from one end to the other. The copper mold is equipped with an extractor that makes only one face of the mold exposed to the liquid melt. The temperatures in the mold are measured by T-type thermocouples at a frequency up to 60 Hz through a data acquisition system. The two columns of thermocouples are spaced 3 and 8 mm away from the mold surface, respectively, as shown in Fig. 1, the dots represent the locations of thermocouples. The arrangement allows the first column of thermocouples to catch the temperature history of the mold that will be used in the minimization of the objective function of the inverse problem. The second column of thermocouple inside the mold wall on $\partial\Omega_4$ (CD) is to provide the temperature boundary condition $f(t)$, where the temperature is interpolated linearly from two near measured temperatures for the nodes in between the two thermocouples at $\partial\Omega_4$. This arrangement of those thermocouples in the mold wall was chosen based on the study of Badri et al. [37] so as to improve the signal-to-noise ratio for the temperature measurements during the experiment. Then, the rectangular area **ABCD** with the height (**AB**) of H (= 21 mm) and the width (**BC**) of W (8 mm) is set as the heat transfer computational domain, which consists of four boundary conditions $\partial\Omega_1$ (DA), $\partial\Omega_2$ (AB), $\partial\Omega_3$ (BC), and $\partial\Omega_4$ (CD).

The experiment runs as follows: Step I The oscillating water-cooling copper mold and the extractor are dipped into the hot melt of liquid steel. After the mold and extractor reached the target depth, the mold flux level and the liquid steel level would be located in the mold thermocouple-measuring zone. Step II The mold and extractor were held for several seconds to form an initial shell on the water-cooled copper mold to ensure the initial shell is strong enough to prevent tearing during extraction. Step III The extractor withdrew the solidifying shell downward at a constant speed to simulate continuous casting. The mold moved upward at a certain speed to compensate for the rise of the mold level, so that the liquid level could be kept in the same position with respect to the mold. Step IV When the casting was completed for the desired length, the mold and extractor were withdrawn out of the furnace and then cooled in air.

By assuming the mold heat transfer is two-dimensional in the vertical section **ABCD** perpendicular to the mold hot surface. The heat transfer within the mold vertical section **ABCD** is assumed to be governed by Fourier partial differential equations. The direct problem, namely the problem of 2D heat transfer within the rectangular area **ABCD**, as shown in Fig. 1, is governed by the following equations.

$$c\rho\frac{\partial T}{\partial t} = \frac{\partial}{\partial x}\left(\lambda\frac{\partial T}{\partial x}\right) + \frac{\partial}{\partial y}\left(\lambda\frac{\partial T}{\partial y}\right), \text{ in domain } \Omega = [0, W] \times [0, H] \qquad (1a)$$
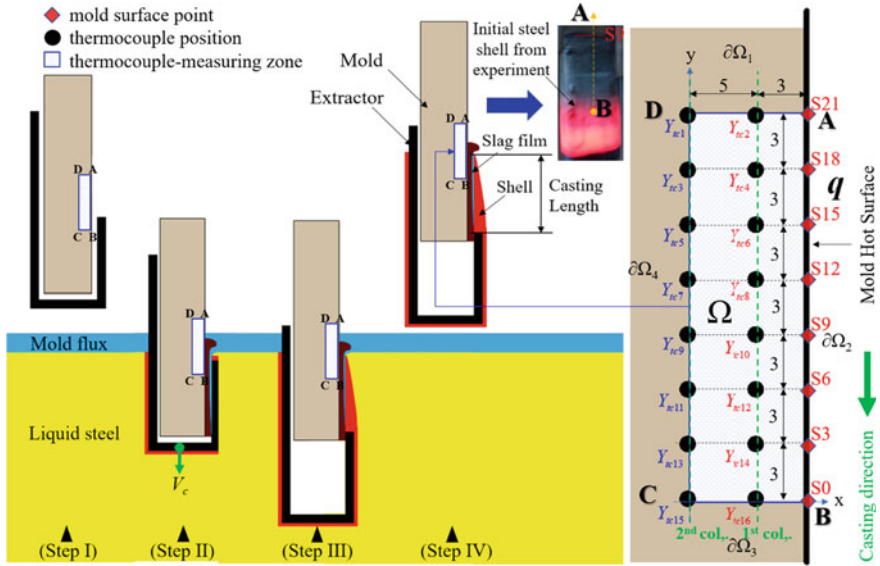
Fig. 1 Computational area of the mold and locations of thermocouples for the casting experiment

$$-\lambda \frac{\partial T(\partial\Omega_1 \cup \partial\Omega_2 \cup \partial\Omega_3, t)}{\partial \boldsymbol{n}} = \boldsymbol{q} \text{ to be estimated.} \tag{1b}$$

$$T(\partial\Omega_4, t) = f(t) \tag{1c}$$

$$T(x, y, 0) = T_{\text{ini}} \tag{1d}$$

where the symbol c represents the specific heat in J kg^{-1}, ρ is the density in kg m^{-3}, T is the temperature in K, t is the time in second, and λ is thermal conductivity in W m^{-1} K^{-1}, q (W m^{-2}) is the heat flux of boundary conditions $\partial\Omega_1$, $\partial\Omega_2$, and $\partial\Omega_3$, $\boldsymbol{n}$ is the outer normal of boundary.

Inverse Problem Description

In this section, the inverse problem is developed based on the function specification method implemented by a spatial Tikhonov regularization [6, 35, 36]. The sequential function specification procedure is: (1) the heat fluxes are assumed to remain constant over the r future time steps, $\boldsymbol{q}^j = \boldsymbol{q}^{j+1} = \cdots = \boldsymbol{q}^{j+r}$, owing to the temperature response is lagging with respect to the boundary heat flux, and (2) By knowing the heat fluxes for $t < t_j$, namely $\tilde{\boldsymbol{q}}^1, \tilde{\boldsymbol{q}}^2, \ldots, \tilde{\boldsymbol{q}}^{j-1}$ are known, estimate $\boldsymbol{q}^j$ so that makes the sum of the squares of the deviations between the calculated temperatures $\mathbf{T}$ and the measured

temperatures $\mathbf{Y}$ in the time interval $[t_j, t_{j+r-1}]$ to be minimized. Then, the inverse heat conduction problem could be converted into a problem that is to estimate $\mathbf{q}^j$ by making the following objective function to be minimum. Therefore, the definition of the inverse heat conduction problem is made as follows

$$s(\boldsymbol{q}^j) = \sum_{k=0}^{r-1} \sum_{m=1}^{M} \left[Y_m^{j+k} - T_m^{j+k}(\boldsymbol{q}^j) \right]^2 + \alpha R(\mathbf{q}^j) \tag{2}$$

where r is the number of future time steps. Y_m^j and T_m^j are the measured temperatures and the calculated temperatures at the time of t_j and the measured position m, respectively. M is the number of sensors. α is the spatial regularization parameter.

The finite difference method is used to solve the above direct problem, where the rectangular area **ABCD** (Ω) will be divided into grids, and the boundaries of $\partial\Omega_1$, $\partial\Omega_2$, and $\partial\Omega_3$ will be split into n_1, n_2, and n_3 divisions, respectively. Then, $\boldsymbol{q}$ has N components, $N = n_1 + n_2 + n_3$, and q_k^j represents the kth component of heat flux $\boldsymbol{q}$ at the time of t_j.

$$\boldsymbol{q}^j = [\boldsymbol{q}_1^j, \boldsymbol{q}_2^j, \boldsymbol{q}_3^j]^{\mathrm{T}}, \boldsymbol{q}_1^j = \left[q_1^j, q_2^j, \ldots, q_{n_1}^j \right]^{\mathrm{T}},$$
$$\boldsymbol{q}_2^j = \left[q_{n_1+1}^j, q_{n_1+2}^j, \ldots, q_{n_1+n_2}^j \right]^{\mathrm{T}} \text{ and}$$
$$\boldsymbol{q}_3^j = \left[q_{n_1+n_2+1}^j, q_{n_1+n_2+2}^j, \ldots, q_N^j \right]^{\mathrm{T}}.$$

Besides, a first-order of spatial Tikhonov regularization term is added to the objective function Eq. (2) so as to improve the spatial stabilization of the solution. It should be mentioned that heat flux $\mathbf{q}$ might be subjected to discontinuity at the intersection points between two adjacent boundaries of $\partial\Omega_1$ and $\partial\Omega_2$ ($\partial\Omega_2$ and $\partial\Omega_3$). Thus, the spatial Tikhonov regularizations for the heat flux of the boundaries $\partial\Omega_1$, $\partial\Omega_2$, and $\partial\Omega_3$ are described separately. That is

$$R(\mathbf{q}^j) = \sum_{n=1}^{n_1-1} (q_n^j - q_{n+1}^j)^2 + \sum_{n=n_1+1}^{n_1+n_2-1} (q_n^j - q_{n+1}^j)^2 + \sum_{n=n_1+n_2+1}^{N-1} (q_n^j - q_{n+1}^j)^2 \tag{3}$$

The estimated temperature $\mathbf{T}^j$ could be evaluated using a Taylor series expansion around the current solution $\tilde{\mathbf{q}}^j$.

$$\mathbf{T}^j = \tilde{\mathbf{T}}(\tilde{\mathbf{q}}^j) + \mathbf{X}_j (\mathbf{q}^j - \tilde{\mathbf{q}}^j). \tag{4}$$

$\tilde{\mathbf{T}}(\tilde{\mathbf{q}}^j)$ is the temperature calculated using the current solution $\tilde{\mathbf{q}}^j$. $\mathbf{X}_j$ is called as the $M \times N$ sensitivity coefficient matrix at time t_j and is defined as follows.

$$\mathbf{X}_j = \left[\frac{\partial \mathbf{T}(\mathbf{q}^j)}{\partial \mathbf{q}^j}\right]^{\mathrm{T}} = \begin{pmatrix} X^j_{1,1} & X^j_{1,2} & \cdots & X^j_{1,N} \\ X^j_{2,1} & X^j_{2,2} & \cdots & X^j_{2,N} \\ \vdots & \vdots & \ddots & \vdots \\ X^j_{M,1} & X^j_{M,2} & \cdots & X^j_{M,N} \end{pmatrix}, \text{ where}$$

$$X^j_{m,n} = \frac{\partial T^j_m}{\partial q^j_n}. \tag{5}$$

The least squares equation $s(\mathbf{q}^j)$ is minimized by differentiating it with respect to each component of unknown heat flux and setting the resulting expressions equal to zero, then a set of N equations is obtained for the estimation of heat flux.

$$\frac{\partial s(\mathbf{q}^j)}{\partial q^j_1} = 0, \ \frac{\partial s(\mathbf{q}^j)}{\partial q^j_2} = 0, \dots, \ \frac{\partial s(\mathbf{q}^j)}{\partial q^j_N} = 0 \tag{6}$$

The above equations yield to a matrix system to estimate the increment for a new heat flux.

$$\Delta \mathbf{q}^j = \left(\sum_{i=1}^{r} \mathbf{X}^T_i \mathbf{X}_i + \alpha \mathbf{H}\right)^{-1} \left(\sum_{i=1}^{r} \mathbf{X}^T_i (\mathbf{Y}^{j+i-1} - \tilde{\mathbf{T}}^{j+i-1})\right) \tag{7}$$

where $\mathbf{H}$ is the $N \times N$ block diagonal regularization matrix. Both $\mathbf{Y}^j$ and $\mathbf{T}^j$ are $M \times 1$ vector, and M is the number of measurements.

$$\mathbf{Y}^j = [Y^j_1, Y^j_2, \dots, Y^j_M]^{\mathrm{T}} \tag{8a}$$

$$\mathbf{T}^j = [T^j_1, T^j_2, \dots, T^j_M]^{\mathrm{T}} \tag{8b}$$

$$\mathbf{H} = \text{blkdiag}(\mathbf{H}_{n_1}, \mathbf{H}_{n_2}, \mathbf{H}_{n_3}) \tag{8c}$$

$$\mathbf{H}_{n_i} = \begin{bmatrix} 1 & -1 & & & \\ -1 & 2 & -1 & & \\ & \ddots & \ddots & \ddots & \\ & & -1 & 2 & -1 \\ & & & -1 & 1 \end{bmatrix}_{n_i \times n_i}. \tag{8d}$$

Sensitivity Coefficient Matrix

$X_{m,n}^{j}$ represents the temperature rise at the sensor location (x_m, y_m) for a unit step change in the surface heat flux at the point (x_n, y_n) of boundaries $\partial\Omega_1$, $\partial\Omega_2$, and $\partial\Omega_3$ and the time t_j. According to the definition of sensitivity coefficient [Eq. (5)], the sensitivity coefficient problem for calculating sensitivity coefficient matrix is obtained by taking the derivative of Eqs. [1a through 1d] with respect to a heat flux component q_n^{j} at the point (x_n, y_n) of boundaries $\partial\Omega_1$, $\partial\Omega_2$, and $\partial\Omega_3$, and n is 1, 2, …, N. The sensitivity coefficient problem governing the sensitivity coefficients $X_{m,n}^{j}$ is

$$c\rho \frac{\partial X_{,n}}{\partial t} = \frac{\partial}{\partial x}\left(\lambda \frac{\partial X_{,n}}{\partial x}\right) + \frac{\partial}{\partial y}\left(\lambda \frac{\partial X_{,n}}{\partial y}\right), \ 0 < t \le t_r$$

$$\text{in domain } \Omega = [0, W] \times [0, H] \tag{9a}$$

$$-\lambda \frac{\partial X_{,n}(\partial\Omega_1 \cup \partial\Omega_2 \cup \partial\Omega_3, t)}{\partial \boldsymbol{n}} = \begin{cases} 1, \ (x, y) = (x_n, y_n) \\ 0, \ \text{others} \end{cases} \tag{9b}$$

$$X_{,n}(\partial\Omega_4, t) = 0 \tag{9c}$$

$$X_{,n}(x, y, 0) = 0 \tag{9d}$$

The Determination of Regularization Parameter

The choice of the regularization parameter is required to balance the computational cost and the stability of the inverse problem solution algorithm. The L-curve method is adopted to optimize the regularization parameters α. L-curve criterion that plotted the curve of $\{\log(\|\mathbf{Y}–\mathbf{T}\|), \log(R(\mathbf{q}^{j}))\}$ often takes on a characteristic L shape, and the optimal regularization parameter was corresponding to the corner of maximum curvature in L-curve [38, 39]. However, many tests should be executed for the plot L-curve, which is very computationally expensive. Alternatively, we consider the use of Arcangeli's discrepancy principle to significantly speed up the selection of the optimal regularization parameter [40], that is

$$\|\mathbf{Y} - \mathbf{T}\| \approx \frac{\sigma}{\sqrt{\alpha}} \tag{10}$$

Stopping Criterion for the Iterative Procedure of Inverse Problem

The stopping criterion for Eq. (2) is given by

$$s \leq \varepsilon \tag{11}$$

As temperatures contain measurement error, the temperature residual could be approximated by

$$\varepsilon = (\mathbf{Y} - \mathbf{T})^{\mathrm{T}}(\mathbf{Y} - \mathbf{T}) \cong M\sigma^2 \tag{12}$$

where σ is the standard deviation of temperature measurement error.

Algorithm of Inverse Problem

As shown in Fig. 2, specify the number of future time steps r. **Step 1**, 2DIHCP is running with an initial guess heat flux $\boldsymbol{q}^j$ and a guess regularization parameter α. **Step 2**, solve the direct problem given by Eq. (1) with the estimated heat flux $\mathbf{q}^j$ for $\mathbf{T}$ during the time from t_j to t_{j+r}. **Step 3**, solve the sensitivity coefficient problem given by Eq. (9a–d) for the sensitivity coefficient matrix $\mathbf{X}$ in the time interval from 0 to t_r. **Step 4**, check the stopping criterion given by Eq. (11). If the stopping criterion Eq. (11) is satisfied, let $\alpha_{\text{old}} = \alpha$ and renew α using Eq. (10). Otherwise, the heat flux is updated using $\boldsymbol{q}^j = \boldsymbol{q}^j + \Delta\boldsymbol{q}$ and Eq. (7), and return to **Step 2**. **Step 5**, when $|\alpha - \alpha_{\text{old}}|/\alpha_{\text{old}} < 0.05$ is satisfied, $\mathbf{q}^j$ could be regarded as the estimated heat flux at time t_j, then set $j = j + 1$ and return to **Step 1** for the next time step calculation till the end of the time steps. Otherwise, the heat flux is updated using $\boldsymbol{q}^j = \boldsymbol{q}^j + \Delta\boldsymbol{q}$ and Eq. (7), and return to **Step 2**. The algorithm is achieved and programed using MATLAB$^{\mathrm{TM}}$. All the partial differential equations are solved using the finite difference method.

Model Verification

Validation for Solving Partial Differential Equations by Numeric Solution

Partial differential equations of heat conduction problems Eqs. [1a through 1d] and the sensitivity coefficient problem given by Eqs. [9a through 9d] are solved using the **f**inite **d**ifference **m**ethod (**FDM**) with the classical Crank-Nicolson (**CN**) semi-implicit scheme. The **FDM** code must be validated to be effective for solving partial

Fig. 2 Algorithm of the
two-dimensional inverse heat
conduction problem
(2DIHCP)
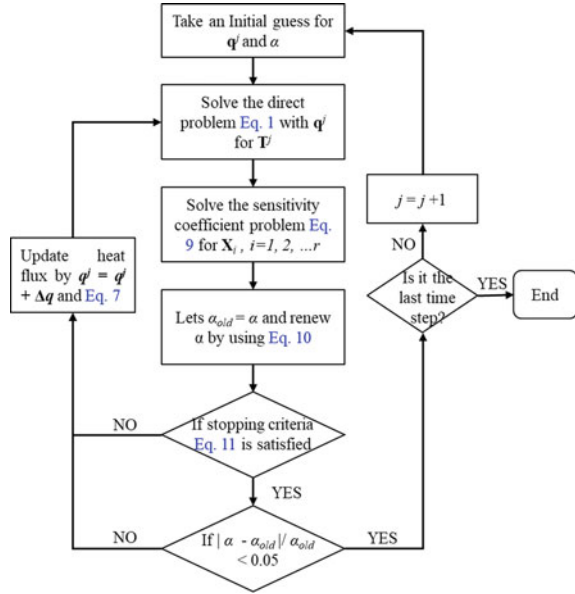
differential equations before the run of the inverse calculation. Herein, the **FDM**
code was also verified through comparison with the analytical solutions of the heat
transfer in the solid from a classical textbook [41]. It was observed that the results
of the **FDM** method were consistent with those analytic solutions, suggesting the
FDM method can solve the heat conduction partial differential equation.

Validation for Algorithm of the Inverse Problem

The numeric test-problem is designed to verify the 2DIHCP. The direct problem is
also a the rectangular area **ABCD** (made of copper, height H is 0.021 m and width
W is 0.008 m, see Fig. 1) with the initial temperature of 273.15 K. The boundaries
of $\partial\Omega_1$, $\partial\Omega_3$, and $\partial\Omega_4$ are insulated boundaries, and the heat flux $f(y, t)$ is applied to
the $\partial\Omega_2$. The $f(y, t)$ is

$$
f(y, t) = \begin{cases} 1 \times 10^6, & 0 \le t < 5 \\ 1 \times 10^6\left(1 - \frac{1000}{21}y\right)\frac{t}{5} + 1 \times 10^6, & 5 \le t < 10 \\ 1 \times 10^6\left(1 - \frac{1000}{21}y\right) + 1 \times 10^6, & 10 \le t < 15 \\ 1 \times 10^6\left(1 - \frac{1000}{21}y\right)\frac{15-t}{5} + 1 \times 10^6, & 15 \le t \le 20 \\ 1 \times 10^6, & 20 \le t < 25 \end{cases} \tag{13}
$$

The first column of eight virtual thermocouples was set 3 mm apart vertically
from each other and 3 mm away from the mold hot surface; while the second column

of other eight virtual thermocouples was spaced 3 mm apart vertically and 8 mm horizontally away from the hot face of the mold. The temperature measurement is taken every 0.1 s during the test-problem runs. The Gaussian noise signals $\sigma\omega$ ($T = T_{\text{ture}} + \sigma\omega$, σ is the standard deviation of noise and ω is a random variable and will be within -2.576 to 2.576 for the 99% confidence bounds) are added to the temperatures to mimic the thermocouple measurement error. Then, the measured temperatures are delivered to the 2DIHCP for the reconstruction of the heat flux in Ω_2. For the parameters used here, the number of future time steps is set as 15, the α is 1.71×10^{-6}, respectively. The estimation results of heat flux in Ω_2 with/without noise (Gaussian noise signals, $\sigma = 0.1$, to simulate the temperature measurement errors) and the exact value *f(y, t)* are shown in Fig. 3, where the heat fluxes at the locations of *y* at 0 mm, 3, 6, 9, 15, and 21 mm are listed, respectively. It was found that the heat fluxes calculated by 2DIHCP match well with the exact values, even for the situation that the measured temperature was contaminated by noise. This suggests that the 2DIHCP could reconstruct the boundary heat flux precisely and show the ability to resist measurement noises.

The results are compared with those values calculated by a robust one-dimensional **i**nverse **h**eat **c**onduction **p**roblem (1D-IHCP) developed by Beck et al. [12], where the future time step is 4. As shown in Fig. 3, although the heat fluxes obtained through 1D-IHCP show the same variation tendency with the exact value, the difference between the above two methods is obvious, especially when the measured temperature is contaminated with noise.

Application to Continuous Casting Mold

A continuous casting experiment of liquid steel ([C]: 0.200 wt%, [Si]: 0.230 wt%, [Mn]: 0.490 wt%, [P]: 0.012 wt%, and [S]: 0.03 wt%) was conducted, where the mold was oscillated with a frequency of 2.17 Hz that helps to separate the metal from the mold. With the progressive filling of the liquid steel (shown in Fig. 1), the responding copper mold wall temperatures were measured by thermocouples with a 60 Hz sampling rate, and the pouring temperature of steel was 1833 K. The calculation domain size and the distribution of the thermocouples are the same as the installation of the thermocouples in the numeric test-problem.

Figure 4 shows the measured in-mold temperature history of the first column thermocouples at different positions in the vertical. The responding temperature can be divided into two stages according to the process of the casting. In stage **I** (51.4–52.5 s), the responding temperatures increase quickly as the progressive filling of the liquid steel from the bottom to the top of the mold. After filling of the melt is completed, the liquid level corresponds to the location S9 with *y* is 9 mm, where the mold is exposed to air above this location (*y* > 9 mm). As it steps into stage **II** (52.5–58 s), the liquid steel is solidified against the surface of the water-cooled mold, the responding temperatures continue to increase and then keep relatively constant. It was found that the steady state temperature values for Y_{tc16} (*y* is 0 mm) and Y_{tc14}
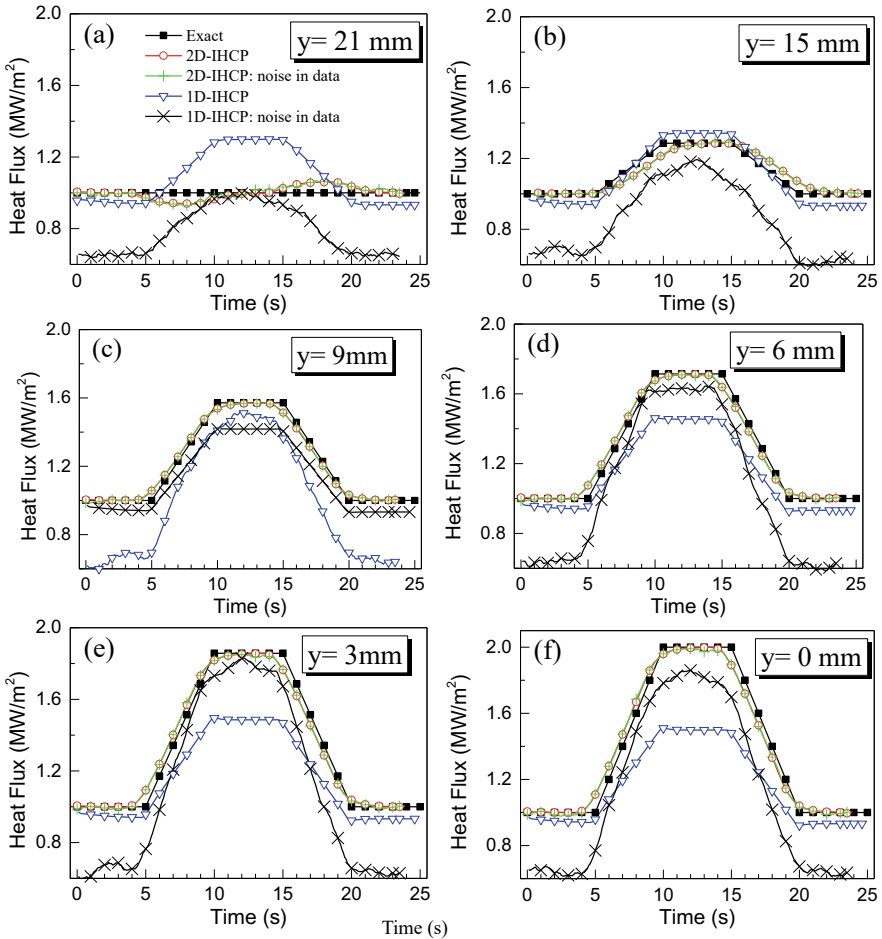
Fig. 3 Heat fluxes calculated by 2DIHCP and 1D-IHCP for the test-problem: **a** heat flux at $y = 21$ mm. **b** heat flux at $y = 15$ mm. **c** heat flux at $y = 9$ mm. **d** heat flux at $y = 6$ mm. **e** heat flux at $y = 3$ mm. **f** heat flux at $y = 0$ mm

(y is 3 mm) are the highest, followed by Y_{tc12} (y is 6 mm), Y_{tc10} (y is 9 mm), Y_{tc8} (y is 12 mm), Y_{tc6} (y is 15 mm), Y_{tc4} (y is 18 mm), and Y_{tc2} (y is 21 mm). It is suggested that the thermocouples corresponding to mold surface exposed to the air are cooler than those of thermocouples below the melt level.

Figure 5 shows the mold heat fluxes calculated by 2DIHCP from measured mold temperatures. For the 2DIHCP runs, the future time step is configured as 8, and α is 7 $\times 10^{-9}$, respectively. During **stage I** of filling, it was found that the local heat fluxes increase rapidly and then reach their peak values and the highest value is around 1.03 MW/m^2, which is similar to industrial and other experimental results [3, 5–8]. During **stage II**, all the heat fluxes decrease rapidly at first due to the fast formation of

Fig. 4 Responding in-mold temperatures
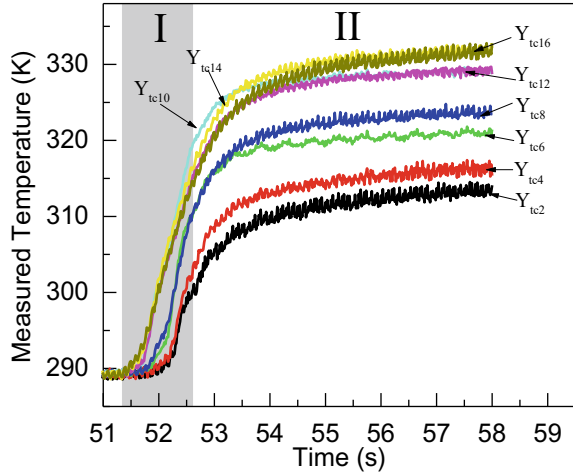
the shell/mold air-gap, and then they continue to decrease gradually. From the above results, it could be suggested that during the initial filling of the liquid steel, the heat fluxes increased dramatically as the hot liquid directly contacted with the cold mold and the latent heat was released greatly with the increase of heat flux in **stage I**. Then, the initial shell is formed against the hot surface of the water-cooling mold; thus, the air gap in between the mold-metal interface is formed due to the solidification of liquid steel and consequently the interfacial thermal resistance increases dramatically, which explains the reason why the heat flux reduces intensively at the initial stage of **stage II**. With the further solidification of the liquid steel, the shell continues to grow and correspondingly the total thermal resistance across the solidified shell and mold-shell interface continues to increase. That is the reason why the heat fluxes were reduced gradually throughout the rest of **stage II**.

In the latter part of **stage II**, the other interesting phenomenon that was observed in this study is that the heat fluxes of locations at S3 (*y* is 3 mm) and S6 (*y* is 6 mm) are the highest, followed by S9 (*y* is 9 mm) and S0 (*y* is 0 mm), then S12 (*y* is 12 mm), S15 (*y* is 15 mm), S18 (*y* is 18 mm), and S21 (*y* is 21 mm). It might be explained that the location of S0 below the liquid steel level S9 (*y* is 9 mm) has a thicker shell thickness due to the longer solidification time, which resulted in a larger thermal resistance than the locations of S3 (*y* is 3 mm) and S6 (*y* is 6 mm), which the finding is consistent with other studies [5–8]. As for the position at the liquid level S9 (*y* is 9 mm), there exists significant vertical heat transfer upward to the top part of the mold, therefore, its heat flux is a little bit smaller than those of S3 and S6. As for the heat fluxes at S12 (*y* is 12 mm), S15 (*y* is 15 mm), S18 (*y* is 18 mm), and S21 (*y* is 21 mm), they are decreasing because they are far away from the liquid melt and the existing vertical heat transfer from the liquid to the upper mold. Therefore, the mold heat transfer is two-dimensional from the location 3 to 6 mm below the liquid melt vertically toward the upper part (may be a little downward) and horizontally to the inside of the mold.

Fig. 5 Mold heat flux calculated by 2DIHCP
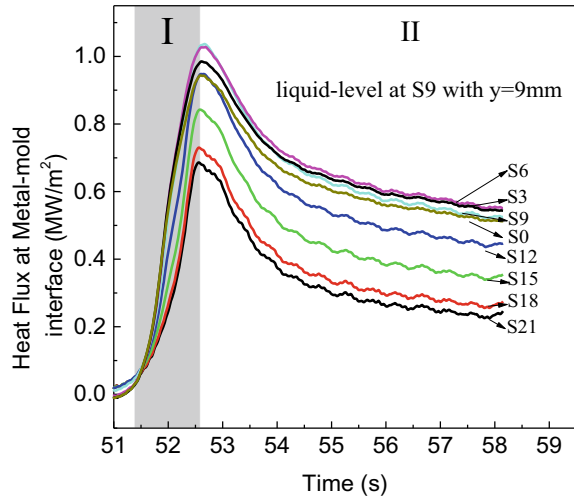
The mold wall temperature evolution during the casting process is reconstructed by 2DIHCP and shown in Fig. 6. The temperatures of the lower part of the mold wall are increased (turns to red) at first with the initial filling of the liquid steel, and then the hot red area expands both horizontally and vertically with the progressive filling of the liquid steel, which indicates the significant 2D heat transfer inside the mold as suggested above. It was noticed that there was no significant evolution of the temperature inside the mold after 54 s, which is consistent with Fig. 4, and the maximum temperature of the mold wall reaches as high as 335 K.

Conclusions

In this work, based on the function specification method with first-order spatial regularization, a two-dimensional transient inverse heat conduction problem (2DIHCP) is established for the determination of the mold heat flux using mold temperatures measured by fast response thermocouples at a frequency up to 60 Hz. The specific conclusions are summarized as:

1. The inverse problem of the function specification method implemented with the first-order spatial regularization could improve the temporal and spatial stabilization of recovered mold heat flux.
2. The built two-dimensional transient inverse heat conduction problem (2DIHCP) could reconstruct the boundary heat flux precisely and is capable of the ability to resist measurement noises. It could also provide more precise heat flux calculation than the one-dimensional **i**nverse **h**eat **c**onduction **p**roblem (1D-IHCP).
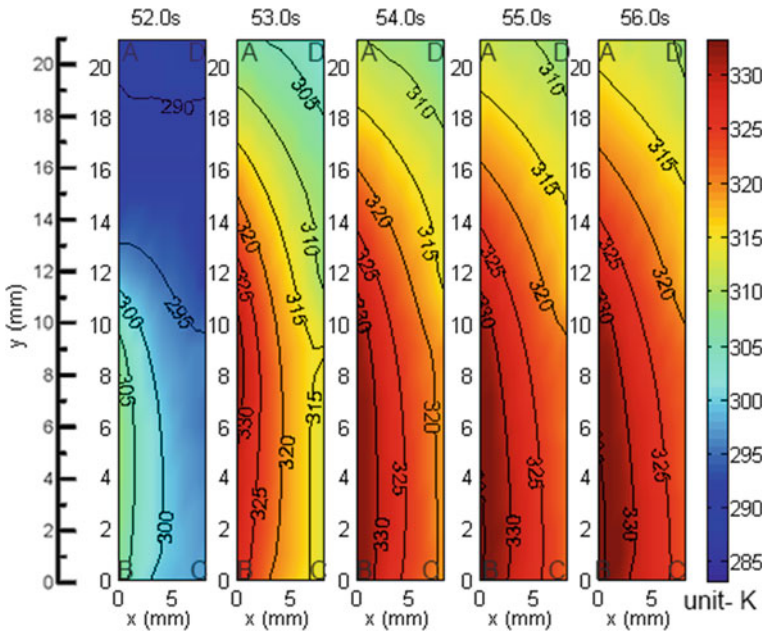
Fig. 6 Temperature evolution of the mold wall during the casting

Conflicts of Interest
The authors declare that they have no conflicts of interest.

References

1. Balogun D, Roman M, Gerald RE, Huang J, Bartlett L, O'Malley R (2022) Shell measurements and mold thermal mapping approach to characterize steel shell formation in peritectic grade steels. Steel Res Int 93(1):2100455
2. Niu Z, Cai Z, Zhu M (2020) Heat transfer behaviour of funnel mould copper plates during thin slab continuous casting and channel structure optimization. Ironmaking Steelmaking 47(10):1135–1147
3. Zhang H, Wang W (2017) Mold simulator study of heat transfer phenomenon during the initial solidification in continuous casting mold. Metall Mater Trans B 48(2):779–793
4. Badri A, Natarajan TT, Snyder CC, Powers KD, Mannion FJ, Byrne M, Cramb AW (2005) A mold simulator for continuous casting of steel: part II. The formation of oscillation marks during the continuous casting of low carbon steel. Metall Mater Trans B 36(3):373–383
5. Zhang H, Wang W (2016) Mold simulator study of the initial solidification of molten steel in continuous casting mold: part II. Effects of mold oscillation and mold level fluctuation. Metall Mater Trans B 47(2):920–931

6. Lyu P, Wang W, Zhang H (2017) Mold simulator study on the initial solidification of molten steel near the corner of continuous casting mold. Metall Mater Trans B 48(1):247–259

7. Zhang H, Wang W, Ma F, Zhou L (2015) Mold simulator study of the initial solidification of molten steel in continuous casting mold. Part I: experiment process and measurement. Metall Mater Trans B 46(5):2361–2373

8. Lopez PER, Mills KC, Lee PD, Santillana B (2012) A unified mechanism for the formation of oscillation marks. Metall Mater Trans B 43(1):109–122

9. Arunkumar S, Rao KS, Kumar TP (2008) Spatial variation of heat flux at the metal–mold interface due to mold filling effects in gravity die-casting. Int J Heat Mass Transf 51(11–12):2676–2685

10. Roman M, Balogun D, Zhuang Y, Gerald RE, Bartlett L, O'Malle RJ, Huang J (2020) A spatially distributed fiber-optic temperature sensor for applications in the steel industry. Sensors 20(14):3900

11. Cardiff M, Kitanidis PK (2008) Efficient solution of nonlinear, underdetermined inverse problems with a generalized PDE model. Comput Geosci 34(11):1480–1491

12. Beck JV, Blackwell B, Clair CR Jr (1985) Inverse heat conduction: Ill-posed problems. James Beck, New York

13. Yu Y, Luo X (2015) Estimation of heat transfer coefficients and heat flux on the billet surface by an integrated approach. Int J Heat Mass Transf 90:645–653

14. Pinheiro CAM, Samarasekera IV, Brimacomb JK, Walker BN (2000) Mould heat transfer and continuously cast billet quality with mould flux lubrication Part 1 Mould heat transfer. Ironmaking Steelmaking 27(1):37–54

15. Thomas BG, Wells MA, Li D (2011) Monitoring of meniscus thermal phenomena with thermocouples in continuous casting of steel. TC 216(416):8900

16. Wang X, Tang L, Zang X, Yao M (2012) Mold transient heat transfer behavior based on measurement and inverse analysis of slab continuous casting. J Mater Process Technol 212(9):1811–1818

17. Chang CW, Liu CH, Wang CC (2018) Review of computational schemes in inverse heat conduction problems. Smart Sci 6(1):94–103

18. Du F, Wang X, Fu J, Han X, Xu J, Yao M (2018) Inverse problem-based analysis on non-uniform thermo-mechanical behaviors of slab during continuous casting. Int J Adv Manufact Technol 94(1):1189–1196

19. Trovant M, Argyropoulos S (2000) Finding boundary conditions: a coupling strategy for the modeling of metal casting processes: part I. Experimental study and correlation development. Metall Mater Trans B 31(1):75–86

20. Griffiths WD (2000) Modelled heat transfer coefficients for Al–7 wt-% Si alloy castings unidirectionally solidified horizontally and vertically downwards. Mater Sci Technol 16(3):255–260

21. Chakraborty S, Ganguly S, Chacko EZ, Ajmani SK, Talukdar P (2017) Estimation of surface heat flux in continuous casting mould with limited measurement of temperature. Int J Therm Sci 118:435–447

22. Li Y, Wang G, Chen H (2015) Simultaneously estimation for surface heat fluxes of steel slab in a reheating furnace based on DMC predictive control. Appl Therm Eng 80:396–403

23. Zhang H, Wang W, Zhou L (2015) Calculation of heat flux across the hot surface of continuous casting mold through two-dimensional inverse heat conduction problem. Metall Mater Trans B 46(5):2137–2152

24. Özisik MN, Orlande HR (2018) Inverse heat transfer: fundamentals and applications. Routledge

25. Zhang L, Li L, Ju H, Zhu B (2010) Inverse identification of interfacial heat transfer coefficient between the casting and metal mold using neural network. Energy Convers Manage 51(10):1898–1904

26. Jayakrishna P, Chakraborty S, Ganguly S, Talukdar P (2021) Modelling of thermofluidic behaviour and mechanical deformation in thin slab continuous casting of steel: an overview. Can Metall Q 60(4):320–349

27. Argyropoulos SA, Carletti H (2008) Comparisons of the effects of air and helium on heat transfer at the metal-mold interface. Metall Mater Trans B 39(3):457–468
28. Kovačević L, Terek P, Kakaš D, Miletić A (2012) A correlation to describe interfacial heat transfer coefficient during solidification of Al–Si alloy casting. J Mater Process Technol 212(9):1856–1861
29. Sun Z, Hu H, Niu X (2011) Determination of heat transfer coefficients by extrapolation and numerical inverse methods in squeeze casting of magnesium alloy AM60. J Mater Process Technol 211(8):1432–1440
30. Rajaraman R, Velraj R (2008) Comparison of interfacial heat transfer coefficient estimated by two different techniques during solidification of cylindrical aluminum alloy casting. Heat Mass Transf 44(9):1025–1034
31. Coates B, Argyropoulos SA (2007) The effects of surface roughness and metal temperature on the heat-transfer coefficient at the metal mold interface. Metall Mater Trans B 38(2):243–255
32. Dour G, Dargusch M, Davidson C (2006) Recommendations and guidelines for the performance of accurate heat transfer measurements in rapid forming processes. Int J Heat Mass Transf 49(11–12):1773–1789
33. Blanc G, Raynaud M, Chau TH (1998) A guide for the use of the function specification method for 2D inverse heat conduction problems. Revue Générale Therm 37(1):17–30
34. Babu K, Prasanna Kumar TS (2010) Mathematical modeling of surface heat flux during quenching. Metall Mater Trans B 41(1):214–224
35. Wang W, Long X, Zhang H, Lyu P (2018) Mold simulator study of effect of mold oscillation frequency on heat transfer and lubrication of mold flux. ISIJ Int 58(9):1695–1704
36. Orlande HR (2012) Inverse problems in heat transfer: new trends on solution methodologies and applications. J Heat Transf 134(3)
37. Badri A, Natarajan TT, Snyder CC, Powers KD, Mannion FJ, Cramb AW (2005) A mold simulator for the continuous casting of steel: part I. The development of a simulator. Metall Mater Trans B 36(3):355–71
38. Aster RC, Borchers B, Thurber CH (2018) Parameter estimation and inverse problems. Elsevier, New York
39. Vogel CR (ed) (2002) Computational methods for inverse problems. Society for Industrial and Applied Mathematics, Philadelphia
40. George S, Thamban Nair M (1998) On a generalized Arcangeli's method for Tikhonov regularization with inexact data. Numer Funct Anal Optim 19(7–8):773–787
41. Özısık MN (ed) (1993) Heat conduction, 2nd edn. Wiley, New York, pp 62–75